Plate/Shell Finite Element for Piezoelectric Patch Modelling

Olivier Polit, Michele d'Ottavio, Philippe Vidal

IX ECCOMAS Thematic Conference on Smart Structures and Materials
SMART 2019
A. Benjeddou, N. Mechbal and J.F. Deü (Eds)

PLATE/SHELL FINITE ELEMENT FOR PIEZOELECTRIC PATCH MODELLING

O. Polit, M. D'Ottavio and P. Vidal

LEME - UPL - Univ. Paris Nanterre
50 rue de Sèvres
92410 Ville d'Avray - France
e-mail: olivier.polit@parisnanterre.fr

Key words: Composite structures, finite element, high-order model, Zig-Zag function, piezoelectric patch analysis

Abstract. This paper presents a C^0 8-node quadrilateral finite element (FE) for geometrically linear piezoelectric plates/shells. It is based on a high-order kinematics proposed in [1] for the mechanical part. The approximation of the electric potential must be able to model piezoelectric patches, and a constant value is considered on each elementary domain while a cubic variation in each layer is used, based on the polynomial expansion given in [2]. Furthermore, Murakami's ZigZag functions [3] is superimposed for the three displacement components for improving the accuracy for multilayered modeling. A plate/shell FE is obtained with nine degrees of freedom (dof) per node for the mechanical part, twelve dofs if the ZigZag functions are included, [4].

This FE is evaluated on some standard piezo-electric plate/shell tests including sensor and actuator configurations. Tests concerning bimorph piezoelectric beam/plate/shell are presented in order to assess the high-order kinematics and the ZigZag effect. The role of electrode segmentation, i.e. the size of equipotential surfaces, on the electro-mechanical response has been also considered.

1 INTRODUCTION

Research and development concerning high-performance structures are very intense since some decades. Structural health monitoring, active vibration damping, and energy harvesting are some examples of possible applications of a multifunctional structural component. Piezoelectric materials permit to convert mechanical and electrical energy at frequency ranges that are most interesting for technical applications such as vibration damping and rapid shape adaptation [5]. Development of theoretical and numerical models for this kind of structures is very important and active. For this purpose and in the framework of two-dimensional plate/shell models, different choices can be made for the mechanical approximation and the following classification is classically admitted for the variation in the thickness direction: (i) Equivalent Single Layer (ESL) models, in which the number of unknowns is independent of the layer number; (ii) Layer-Wise (LW) descriptions, for which the number of unknowns and, thus, the computational cost increases with the number of layers. While most developments employ an ESL description for the mechanical behavior, and particularly the First order Shear Deformation Theory (FSDT), a Layer-Wise description is necessary for the piezoelectric approximation to impose electric boundary conditions at each piezoelectric layer interfaces, i.e., the electrodes, within the stack. Inside each piezoelectric layer, the electric potential can be linear, quadratic or higher and a comparison has been proposed in [6].

A review of different approaches is available in [7, 8] and in the framework of the Carrera Unified Formulation (CUF) in [9]. For the FE approximations, a recent review limited to shell models is also given in [10].

The limitation of the FSDT model is related to the constant transverse displacement hypothesis, inducing no thickness change and the use of the reduced 2D constitutive law. The use of the full 3D constitutive law is an important feature for a consistent representation of complex physical interactions like multi-field coupling. Furthermore, accurate modeling of thick structures needs the transverse normal stress and the 3D constitutive law.

Therefore, a high-order model is chosen with sinus function for the in-plane displacements and quadratic assumption along the thickness of the transverse deflection. Thus, the 3D constitutive law is retained and a parabolic distribution of the transverse shear strains and a non linear variation of the transverse normal strain are recovered. In order to introduce transverse strain discontinuities required to fulfill the interlaminar equilibrium, Murakami's Zig-Zag function (MZZF) [3] is superimposed to the high-order ESL kinematics for the 3 displacement components. Note that MZZF does not depend on the constitutive coefficients and is, hence, attractively simple in conjunction with three-dimensional constitutive laws including multi-field coupling. Based on this kinematics, an 8-node plate Finite Element (FE) is proposed, free of numerical illness such as transverse shear and Poisson lockings, oscillation and spurious mechanics [1]. The approximation of the electric potential must be able to model piezoelectric patches, and a constant value is considered on each elementary domain while a cubic variation in each layer is used, based on the polynomial expansion given in [2, 11].

The paper is organized as follows: Section 2 describes the plate problem, the approximations for the displacement and the electric potential and the system to be solved. The resulting FE are evaluated in Section 3 for a composite plate, in order to talk about the electrode segmentation modelling.

2 Description of the plate problem

2.1 Governing equations

Let us consider a plate occupying the domain $\mathcal{V} = \Omega \times [-\frac{e}{2} \leq z \leq \frac{e}{2}]$ in a Cartesian coordinate system $(x_1, x_2, x_3 = z)$. The plate is defined by an arbitrary surface Ω in the (x_1, x_2) plane, located at the midplane for $z = 0$, and by a constant thickness e.

The displacement is denoted $\vec{u}(x_1, x_2, z)$ and the electric potential is $\phi(x_1, x_2, z)$. $\varepsilon_{ij}(x_1, x_2, z)$ and $\vec{E}(x_1, x_2, z)$ are the strain tensor components and the electric field vector, respectively, deduced from primal variables by the geometric relations. Furthermore, $\sigma_{ij}(x_1, x_2, z)$ and $\vec{D}(x_1, x_2, z)$ are the conjugated fluxes (stress tensor components and dielectric displacement vector, respectively) obtained from the constitutive equations given in the next subsection.

2.1.1 Constitutive relation

The 3D constitutive equation for a linear piezoelectric material is given by the following set of coupled equations [12] for a layer (k):

$$[\sigma^{(k)}] = [C^{(k)}]\,[\varepsilon^{(k)}] - [e^{(k)}]^T\,[E^{(k)}] \tag{1a}$$

$$[D^{(k)}] = [e^{(k)}]\,[\varepsilon^{(k)}] + [\varepsilon^{(k)}]\,[E^{(k)}] \tag{1b}$$

where we denote by $[C]$ the matrix of elastic stiffness coefficients taken at constant electric field, by $[e]$ the matrix of piezoelectric stress coefficients and by $[\varepsilon]$ the matrix of electric permittivity coefficients taken

at constant strain. The explicit form of these matrices can be found in [10] for an orthotropic piezoelectric layer polarized along the thickness direction z. Eq. (1a) expresses the piezoelectric *converse* effect for actuator applications, whereas Eq. (1b) represents the piezoelectric *direct* effect which is exploited in sensor applications. Note that the constitutive law is expressed in the local reference frame associated to each layer.

2.1.2 The weak form of the boundary value problem

The classical piezoelectric variational formulation of [13] is employed in which the primary field variables are the "generalized displacements", i.e. the displacement field, and the electrostatic potential. Using a matrix notation and for admissible virtual displacements $\vec{u}^*$ and electric potential ϕ^* (virtual quantities are denoted by an asterisk), the variational principle is given by:

$$\begin{aligned}\int_{\mathcal{V}} \rho [u^*]^T [\ddot{u}]\, d\mathcal{V} = &- \int_{\mathcal{V}} [\varepsilon(u^*)]^T [\sigma(u,\phi)]\, d\mathcal{V} + \int_{\mathcal{V}} [u^*]^T [f]\, d\mathcal{V} + \int_{\partial\mathcal{V}_F} [u^*]^T [F]\, d\partial\mathcal{V} \\ &+ \int_{\mathcal{V}} [E(\phi^*)]^T [D(u,\phi)]\, d\mathcal{V} - \int_{\mathcal{V}} q\, \phi^*\, d\mathcal{V} - \int_{\partial\mathcal{V}_Q} Q\, \phi^*\, d\partial\mathcal{V}\end{aligned} \tag{2}$$

where $[f]$ is the body force vector, $[F]$ the surface force vector applied on $\partial\mathcal{V}_F$, q the volume charge density, Q the surface charge density supplied on $\partial\mathcal{V}_Q$ and ρ is the mass density. Finally, $\varepsilon(u^*)$ and $E(\phi^*)$ are the virtual strain and virtual electric field that satisfy the compatibility gradient equations. In the remainder of this article we will refer only to static problems, for which the left-hand side term is set to zero. Furthermore, body forces and volume charge densities will be discarded ($[f] = [0]$; $q = 0$).

2.2 The mechanical part

2.2.1 The displacement field

Based on the sinus model, see [14], a new plate model which takes into account the transverse normal stress is presented in this section. This extension is based on following developments

- various models for beams, plates and shells based on the refined sinus theory, see [14, 15, 16, 17, 18, 19];
- our previous paper on a 7 parameter model for thermo-mechanical analysis [1].

In the framework of ESL approach, the kinematics of our model is assumed to have the following particular form

$$\left\{\begin{array}{lcl} U_1(x_\alpha,z) &=& u^0{}_1(x_\alpha) + z\, u^1{}_1(x_\alpha) + f(z)\, u^f{}_1(x_\alpha) \\ U_2(x_\alpha,z) &=& u^0{}_2(x_\alpha) + z\, u^1{}_2(x_\alpha) + f(z)\, u^f{}_2(x_\alpha) \\ U_3(x_\alpha,z) &=& u^0{}_3(x_\alpha) + z\, u^1{}_3(x_\alpha) + z^2\, u^2{}_3(x_\alpha) \end{array}\right. \tag{3}$$

where $\alpha \in \{1,2\}$ and $i \in \{1,2,3\}$. In Eq. (3), the superscript is associated to the expansion order in z while the subscript is related to the component of the displacement. Thus, $u^0{}_i$ are the displacements of a point of the reference surface while $(u^1{}_\alpha, u^f{}_\alpha)$ are measures for rotations of the normal transverse fiber about the axis $(0, x_\alpha)$. The functions $u^\alpha{}_3$ permit to have a non-constant deflection for the transverse fiber and allow to have non zero transverse normal stretch. Furthermore, the quadratic assumption for the transverse displacement avoids the occurrence of Poisson (or thickness) locking, see [1].

In the context of the sinus model, we have

$$f(z) = \frac{e}{\pi} \sin \frac{\pi z}{e} \tag{4}$$

It must be noticed that the classical homogeneous sinus model [14] can be recovered from Eq. (3) assuming ${u^1}_\alpha = -{u^0}_{3,\alpha}$, and neglecting the unknown functions ${u^\alpha}_3$.

2.2.2 The Murakami's Zig-Zag terms

In order to evaluate the influence of Zig-Zag terms [3] in a high-order ESL model, the following displacement per layer (k) are added to Eq. (3):

$$\left\{\begin{array}{lcl} {U_1}^{(k)}(x_\alpha,z) & = & Z^{(k)}(z)\,{u^z}_1(x_\alpha) \\ {U_2}^{(k)}(x_\alpha,z) & = & Z^{(k)}(z)\,{u^z}_2(x_\alpha) \\ {U_3}^{(k)}(x_\alpha,z) & = & Z^{(k)}(z)\,{u^z}_3(x_\alpha) \end{array}\right. \tag{5}$$

with

$$Z^{(k)}(z) = (-1)^k\,\zeta_k(z) \quad \text{and} \quad \zeta_k(z) = \frac{2}{e_k}\left(z - \frac{1}{2}(z_k + z_{k+1})\right) \tag{6}$$

where e_k is the thickness of the k^{th} layer while (z_k, z_{k+1}) are the bottom and top coordinates of this layer. It is obvious that $Z^{(k)}(z)$ is a piecewise linear function with bi-unit amplitude for all the layers as we have $\zeta_k(z) \in [-1,1]$. Note that, despite the $Z^{(k)}(z)$ function depends on the layer index inside the stack, the amplitudes ${u^z}_i$ are unique for the whole laminate, i.e., the ESL framework is still preserved.

2.3 The electric part

On each elementary domain Ω_e, the electric potential is assumed to be constant. Therefore, no variation with respect to x_α is considered. A cubic layerwise (LW) description is used across the thickness, according to the approximation introduced in [2] and used in [11]: In each layer (k), the electric potential distribution is described by the normal electric field components at the bottom and top surfaces, denoted E_{3b} and E_{3t}, respectively, and the potential difference $\Delta\phi$ between top and bottom surface. Using these dofs, the approximation of the electric potential can be written as:

$$\left[\phi^{(k)}\right] = \left[F_\phi\right]\,\left[Cst_\phi^{(k)}\right]\,\left[{q^e}_\phi^{(k)}\right] \tag{7}$$

where the following definitions have been introduced:

$$\left[F_\phi\right] = \left[\begin{array}{cccc} 1 & z & z^2 & z^3 \end{array}\right]; \quad \left[{q^e}_\phi^{(k)}\right]^T = \left[\begin{array}{ccc} {E_{3b}}^{(k)} & \Delta\phi^{(k)} & {E_{3t}}^{(k)} \end{array}\right] \tag{8}$$

and $\left[{Cst_\phi}^{(k)}\right]$ is a (4×3) matrix containing constant coefficients. The electric field vector in each layer $\left[E^{(k)}\right]$ is then obtained as:

$$\left[E^{(k)}\right] = \left[\begin{array}{c} 0 \\ 0 \\ -\phi_{,3}^{(k)} \end{array}\right] = \left[F_E\right]\,\left[{Cst_E}^{(k)}\right]\,\left[{q_\phi}^{e(k)}\right] \text{ with } \left[F_E\right] = \left[\begin{array}{ccc} 1 & z & z^2 \end{array}\right] \tag{9}$$

where $\left[{Cst_E}^{(k)}\right]$ is a (3×3) matrix. So, the adopted approximation yields a quadratic transverse electric field across the thickness of each layer.

2.4 The system to be solved

The FE approximations are not detailed here for the sake of brevity and can be found elsewhere [10, 1]. The eight-node quadrilateral finite element is used and classical FE approximation is used for the geometry. A special treatment is used to control the transverse shear locking by using a dedicated interpolation for ${\gamma_{\alpha 3}}^0$ according to the methodology presented in [1]. Note that since the electric potential is assumed to be constant on each elementary domain, there is no need to introduce any FE approximation for this field.

The elementary matrices are then deduced considering the bi-dimensional weak form obtained from Eq. (2). Assembling each elementary contribution in the global reference frame, the following discrete form of the coupled piezoelectric system is obtained:

$$\begin{bmatrix} [K_{uu}] & [K_{u\phi}] \\ [K_{u\phi}]^T & [K_{\phi\phi}] \end{bmatrix} \begin{bmatrix} [q_u] \\ [q_\phi] \end{bmatrix} = \begin{bmatrix} [L_u] \\ [L_\phi] \end{bmatrix} \tag{10}$$

where $[K_{uu}]$, $[K_{\phi\phi}]$ and $[K_{u\phi}]$ are the global stiffness, dielectric and piezoelectric matrices of the plate, respectively. The mechanical dofs are in the vector $[q_u]$, while the electrical dofs are in the vector $[q_\phi]$ and we have at the elementary level

$$\begin{aligned} [{q_u}^e] &= \left[\left(\begin{array}{ccc|ccc|ccc|ccc} {u^0}_1 & {u^0}_2 & {u^0}_3 & {u^1}_1 & {u^1}_2 & {u^1}_3 & {u^f}_1 & {u^f}_2 & {u^2}_3 & {u^z}_1 & {u^z}_2 & {u^z}_3 \end{array} \right)_{i=1,8} \right] \\ [{q_\phi}^e] &= \left[\left(\begin{array}{ccc} {E_{3b}}^{(k)} & \Delta\phi^{(k)} & {E_{3t}}^{(k)} \end{array} \right)_{k=1,Nl} \right] \end{aligned} \tag{11}$$

with Nl the number of layers. From the mechanical point of view, the Zig-Zag dofs can be activated or not and comparisons will be presented in the next section dedicated to numerical evaluations using no Zig-Zag dof (P9), using only in-plane Zig-Zag dof ${u^z}_\alpha$ (P9Z) and with all the Zig-Zag dof ${u^z}_i$ (P9ZZ). Finally, the three models use 9, 11 or 12 kinematical unknown functions and the associated FE has 72, 88, 96 mechanical dofs per element, respectively.

Since the electric potential is assumed constant on each FE, the assembly involves only the approximation along the thickness. A piezoelectric patch comprising several FEs can be defined through the imposition of the equipotential condition between electrodes: the same $\Delta\phi$ is imposed on the piezoelectric layer for all elements belonging to the same patch. From the numerical point of view, this is accomplished through linear homogeneous and non-homogeneous Multi-Point Constraints (MPC) using penalty function method.

In Eq. (10), the load vectors $[L_u]$ and $[L_\phi]$ represent the external loading from applied forces and prescribed charges, respectively. Essential boundary conditions (i.e., prescribed displacements and electric potentials) are imposed numerically by a penalty technique. The coupled system is then solved by the classical static condensation procedure for the electrical dof:

$$[q_\phi] = [K_{\phi\phi}]^{-1}([L_\phi] - [K_{u\phi}]^T[q_u]) \tag{12a}$$

which yields the following purely mechanical system with a modified equivalent stiffness matrix:

$$\left[[K_{uu}] - [K_{u\phi}][K_{\phi\phi}]^{-1}[K_{u\phi}]^T\right][q_u] = [L_u] - [K_{u\phi}][K_{\phi\phi}]^{-1}[L_\phi] \tag{12b}$$

In the remainder of the paper, $[L_\phi] = [0]$ will be considered.

3 Numerical results: clamped composite plate

This test is interesting to evaluate the segmentation of a piezoelectric layer using different number of patches. It considers the sensory response of a cantilever, rectangular, hybrid sandwich plate with one edge clamped and other edges free subjected to a uniform pressure load according to the following data [20]:

geometry rectangular plate $a \times b$ with $a = 10\ mm$, $a/b = 2$ and total thickness $e = 1\ mm$ (length-to-thickness ratio $S = 10$)

materials seven-layers plate $(pz, 0°, 90°, core, 90°, 0°, pz)$; the outer piezoelectric layers of thickness $0.1\ e$ are made out of PZT-5A material; each layer constituting the laminated skins has a thickness $0.04\ e$ and the core thickness equals $0.64\ e$. The material properties for PZT-5A, skin layers and core are given in Tab. 1

boundary conditions clamped at $x_1 = 0$; uniform pressure load p_0; piezoelectric layers can be in open circuit ($\Delta\phi$ let free) or in closed circuit ($\Delta\phi = 0$)

mesh three regular meshes 5×2, 10×4 and 20×8 are used

results and locations transverse displacement at the tip and piezoelectric potential in the element close to the clamped edge. They are made non-dimensional according to

$$\overline{u}_3 = u_3 \left(10^2 E_2{}^{(core)}\right) / \left(e\, S^4\, p_0\right) \quad \text{with } d_0 = 374\ 10^{-12}\ CN^{-1}$$
$$\overline{\phi} = \phi \left(10^4 E_2{}^{(core)}\, d_0\right) / \left(e\, S^2\, p_0\right)$$

Prop.	PZT-5A	skin	core	Prop.	PZT-5A	skin	core
E_1 [GPa]	61.0	172.5	0.276	e_{15} [C/m^2]	12.3	0	0
E_2 [GPa]	61.0	6.9	0.276	e_{24} [C/m^2]	12.3	0	0
E_3 [GPa]	53.2	6.9	3.45	e_{31} [C/m^2]	-7.2	0	0
ν_{23}	0.38	0.25	0.02	e_{32} [C/m^2]	-7.2	0	0
ν_{13}	0.38	0.25	0.02	e_{33} [C/m^2]	15.1	0	0
ν_{12}	0.35	0.25	0.25	ε_{11} [nF]	15.3	ε_0	ε_0
G_{23} [GPa]	21.1	1.38	.414	ε_{22} [nF]	15.3	ε_0	ε_0
G_{13} [GPa]	21.1	3.45	.414	ε_{33} [nF]	15.	ε_0	ε_0
G_{12} [GPa]	22.6	3.45	0.1104				

Table 1: Material properties employed in the considered problems.

This test can be used to compare the effect of the electrode segmentation: using the proposed FE meshes, the electrode sensor surface is subdivided in 1, 10, 40, 160 patches through the imposition of equipotential conditions.

Tab. 2 presents the convergence properties of the P9 FE when only one patch is used for each piezoelectric layer. In the open circuit configuration, the equipotential condition enforces $\Delta\phi$ in each layer to be the same for all elements. In the closed circuit condition, $\Delta\phi = 0$ for all elements (equipotential condition) and the maximum electric potential value inside the piezoelectric layers is reported. Note that the cubic approximation for ϕ allows to recover the electric potential induced by the local bending of the piezoelectric layers.

elec BC	mesh	5×2	10×4	20×8
OC	$\overline{u}_3$	22.649 (-1.9)	22.967 (-0.5)	23.089
	$\overline{\Delta\phi}_{bottom}$	-23.003 (-2.7)	-23.408 (-1.0)	-23.649
	$\overline{\Delta\phi}_{top}$	24.473 (-2.6)	24.886 (-1.0)	25.129
CC	$\overline{u}_3$	23.370 (-1.9)	23.698 (-0.3)	23.833
	$\overline{\phi}_{Max}$	-3.307	-5.212	-7.295

Table 2: Clamped composite plate with only one electric patch: convergence results for open circuit (OC) and closed circuit (CC).

The maximum displacement is located at the center of the tip edge $(a, b/2)$ while the maximum induced electric potential (ϕ_{max} for closed circuit) is in the FE close to the clamped edge. For the open circuit, the convergence is very fast for both displacement and electric potential difference – the percentage of error with respect to the 20×8 mesh results is indicated in parentheses. For the closed circuit, an asymptotic value is recovered for the displacement whereas ϕ_{max} still increases with mesh refinement; this is due to the decreasing size of the FE at the clamp, which increasingly localizes the bending deformation of the piezoelectric layers.

The distribution of the electric potential across the thickness is illustrated for the two electric boundary conditions in Fig. 1. The non-linear variation across the bottom and top piezoelectric layers is visible on both graphs and increases with mesh refinement. Due to the equipotential condition, it has no influence on the $\Delta\Phi_{max}$ for the open circuit (left) but it is directly related to the Φ_{max} for the closed circuit (right). This non-linear effect measures the local bending deformation of the piezoelectric layers and is accordingly larger at the clamped edge than at the free tip of the plate.

Finally, the effect of electrode segmentation is discussed in Tab. 3 for the open circuit boundary condition. The corresponding distribution along the length of the plate of the electric potential difference is illustrated in Fig. 2 for all considered meshes and electrode segmentations. The induced potential difference $\Delta\phi$ reported in Tab. 3 is taken at the electrode next to the clamped edge, i.e., where it has its maximum value. Comparing the results for 10 patches obtained with two different meshes allows to appreciate the role of the mesh refinement: a finer mesh increases the tip displacement and enhances the sensed voltage. The same mesh with 10×4 elements is then used with two different number of electric patches, i.e., with different sizes of the equipotential surfaces: a very small influence on the tip deflection can be seen, with $\overline{u}_3$ slightly larger when the equipotential surfaces are larger; on the contrary, the electric potential induced at the clamped edge is clearly higher the smaller the electrode. Finally, considering the 20×8 with 160 patches (i.e., one electrode per FE), the tip displacement is slightly higher due to the refined mesh and the sensed voltage is further increased due to both, the larger deflection and the reduced electrode's size at the clamp.

4 Conclusion

This paper has presented a new family of FE for piezoelectric composite plates. A high-order ESL kinematic model is considered that includes the sinus function for the in-plane displacements, a quadratic polynomial expansion for the transverse displacement and Zig-Zag functions for introducing slope discontinuities at layers' interfaces for both, the in-plane and the transverse displacements. A LW cubic approximation is used for the electric potential in order to capture its non-linear distribution induced by the local bending of the piezoelectric layer; the elementary domain is considered as an equipotential surface (constant electric potential).

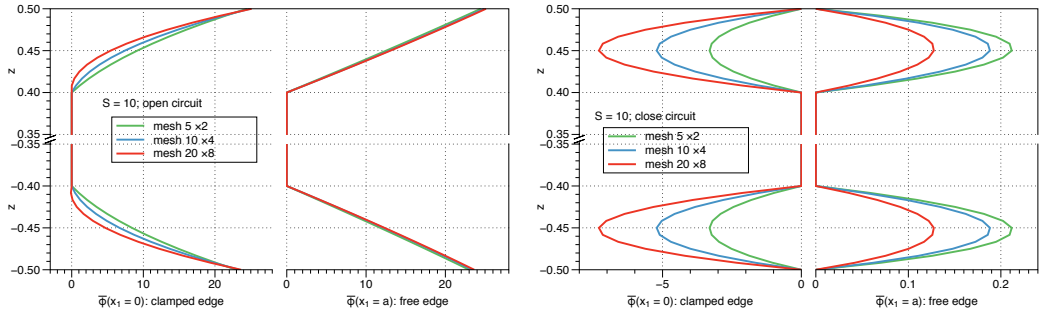

Figure 1: Clamped composite plate: electric potential distribution across the thickness for the OC (left) and CC (right) electric boundary conditions.

patch Nb	10		40	160
mesh	5×2	10×4	10×4	20×8
$\overline{u}_3$	22.230	22.533	22.510	22.609
$\overline{\Delta\phi}_{bottom}$	-62.776	-63.503	-80.004	-91.988
$\overline{\Delta\phi}_{top}$	64.071	64.827	81.147	92.884

Table 3: Clamped composite plate in OC configuration: evaluations for different FE meshes and equipotential surface sizes.

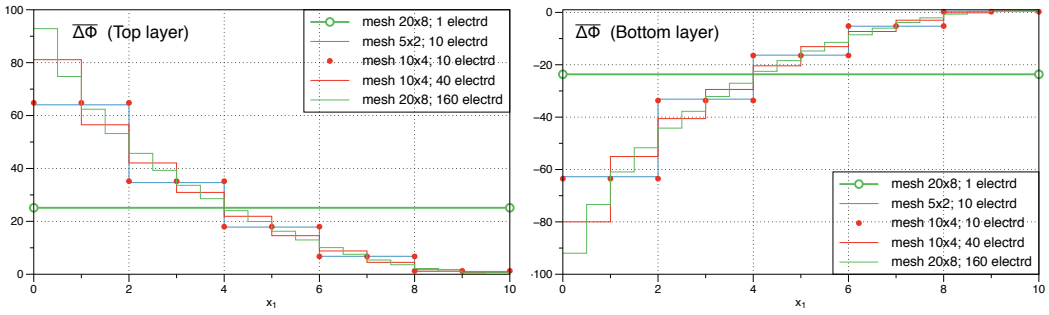

Figure 2: Clamped composite plate in OC configuration: distribution along the length of the sensed voltage at the top (left) and bottom (right) piezoelectric layer for different meshes and electrode segmentation.

The element has been validated through linear static case studies for both sensor and actuator configurations as well as homogeneous and laminated plates. The role of electrode segmentation, i.e., the size of equipotential surfaces, on the electro-mechanical response has been also evaluated. The results are in good agreement for actuator and sensor configurations for thin to very thick cases. The proposed P9ZZ FE, using only 12 mechanical dof per node, is very accurate, simple to use, without any numerical problem and could be used for a large range of plate problems involving piezoelectric patches or layers. Future works are pointed towards the extension of this model to piezoelectric shell structures.

REFERENCES

[1] O. Polit, P. Vidal, M. D'Ottavio, Robust c^0 high-order plate finite element for thin to very thick structures: mechanical and thermo-mecanical analysis, International Journal for Numerical Methods in Engineering 90 (4) (2012) 429–451, dOI: 10.1002/nme.3328.

[2] J. Jiang, D. Li, A new finite element model for piezothermoelastic composite beam, J. Sound Vibr. 306 (2007) 849–864.

[3] H. Murakami, Laminated composite plate theory with improved in-plane response, J. App. Mech. 53 (1986) 661–666.

[4] O. Polit, M. D'Ottavio, P. Vidal, High-order plate finite elements for smart structure analysis, Composite Structures 151 (2016) 81–90.

[5] I. Chopra, Review of state of art of smart structures and integrated systems, AIAA Journal 40 (2002) 2145–2187.

[6] O. Polit, I. Bruant, Electric potential approximations for an eight node plate finite element, Computers and Structures 84 (22-23) (2006) 1480–1493.

[7] S. Gopinathan, V. Varadan, V. Varadan, A review and critique of theories for piezoelectric laminates, Smart Materials and Structures 9 (1) (2000) 24–48.

[8] R. Gibson, A review of recent research on mechanics of multifunctional composite materials and structures, Compos. Struct. 92 (2010) 2793–2810.

[9] E. Carrera, M. Boscolo, A. Robaldo, Hierarchic multilayered plate elements for coupled multifield problems of piezo- electric adaptive structures: formulation and numerical assessment, Archives of Computational Methods in Engineering 14 (4) (2007) 383–430.

[10] P. Vidal, M. D'Ottavio, M. Ben Thaïer, O. Polit, An efficient shell finite element for the static response of piezoelectric laminates, Journal of Intelligent Material Systems and Structures 22 (7) (2011) 671–690.

[11] S. B. Beheshti-Aval, M. Lezgy-Nazargah, P. Vidal, O. Polit, A refined sinus finite element model for the analysis of piezoelectric-laminated beams, Journal of Intelligent Material Systems and Structures 22 (3) (2011) 203–219.

[12] A. S. 176, IEEE Standard on Piezoelectricity, American National Standard Institute, 1987.

[13] H. Tiersen, Linear Piezoelectric Plate Vibrations, Plenum, New-York, 1969.

[14] M. Touratier, An efficient standard plate theory, Int. J. Eng. Sci. 29 (1991) 901–916.

[15] M. Ganapathi, B. P. Patel, P. Boisse, O. Polit, Flexural loss factors of sandwich and laminated composite beams using linear and nonlinear dynamic analysis, Composites Part B: Engineering 30 (3) (1999) 245–256.

[16] O. Polit, M. Touratier, A multilayered/sandwich triangular finite element applied to linear and non-linear analyses, Composite Structures 58 (1) (2002) 121–128.

[17] F. Dau, O. Polit, M. Touratier, C1 plate and shell finite elements for geometrically nonlinear analysis of multilayered structures, Computers and Structures 84 (19-20) (2006) 1264–1274.

[18] P. Vidal, O. Polit, A thermomechanical finite element for the analysis of rectangular laminated beams, Finite Elements in Analysis and Design 42 (10) (2006) 868–883.

[19] P. Vidal, O. Polit, A family of sinus finite elements for the analysis of rectangular laminated beams, Composite Structures 84 (1) (2008) 56–72.

[20] S. Kapuria, S. Kulkarni, Static electromechanical response of smart composite/sandwich plates using an efficient finite element with physical and electric nodes, Int. J. of Mech. Sci. 51 (2009) 1–20.